PowerTrace: Fine-Grained Localization with Wireless-Charging Discovery Signals

Yimeng Liu
Department of Computer Science and Engineering
University of California, Merced
Merced, CA, USA
yliu327@ucmerced.edu

Rahul Sidramappa Hoskeri
Department of Computer Science and Engineering
University of California, Merced
Merced, CA, USA
rhoskeri@ucmerced.edu

Hua Huang
Department of Computer Science and Engineering
University of California, Merced
Merced, CA, USA
hhuang80@ucmerced.edu

***Abstract*—Commodity Qi wireless chargers and reverse-charging smartphones emit low-frequency discovery pings to detect nearby receivers. We present PowerTrace, a system that repurposes these pings for short-range localization without modifying transmitter hardware or charging protocols. PowerTrace captures pings with a compact magnetic receiver and separates concurrent transmitters through period-aligned averaging to extract transmitter-specific signal-strength features. It estimates position by matching these measurements to a physics-informed neural network that models the asymmetric, hardware-dependent fields of commodity chargers. We evaluate three operating modes: probe mode for tagged-object localization using fixed chargers, listen mode for unmodified-phone localization using fixed receivers, and peer-to-peer mode for phone-to-phone ranging using a phone-mounted receiver. In a controlled 100 cm $\times$ 50 cm $\times$ 50 cm workspace, PowerTrace achieves median 3D errors of 5.3 cm in probe mode and 4.1 cm in listen mode, with corresponding 90th-percentile errors of 11.3 cm and 9.9 cm. We evaluate peer ranging over separations of 10–70 cm, with accuracy degrading near the upper end. These results demonstrate that compatible wireless-charging devices can serve as opportunistic magnetic beacons for localization in calibrated, short-range workspaces.**

***Index Terms*—Indoor localization; Qi wireless charging; magnetic sensing; physics-informed neural networks.**

I. Introduction

Locating everyday objects with centimeter-scale accuracy remains challenging indoors. Tasks such as finding an item on a shelf, tracking a phone across a desk, or measuring the separation between nearby smartphones demand fine-grained sensing over short distances, often in cluttered or occluded environments. Existing indoor localization systems based on RFID, BLE, Wi-Fi, UWB, cameras, and acoustic sensing have made substantial progress [1], [2]. Depending on the sensing modality, however, these systems may require dedicated infrastructure or line-of-sight visibility, or provide only coarse-grained, meter-level accuracy. These limitations constrain their deployment in compact, cluttered workspaces, where localization must be accurate, inexpensive, and unobtrusive.

This paper investigates how commodity wireless-charging devices can be repurposed as opportunistic magnetic beacons for short-range localization. Wireless chargers are increasingly embedded in desks, vehicles, furniture, and public spaces, while smartphones equipped with reverse wireless charging can also serve as power transmitters. Our key insight is that the discovery pings emitted by these devices encode spatial information: the magnetic-field strength measured by a nearby receiver varies with their relative position. By exploiting these signals, we achieve centimeter-scale localization without modifying commodity transmitter hardware or the existing charging protocol, enabling a low-cost and unobtrusive solution. Moreover, low-frequency magnetic fields have large skin depths and can penetrate common nonmetallic obstacles such as wood, paper, and plastic, reducing reliance on line-of-sight visibility and susceptibility to multipath in cluttered environments. Together, these properties make it possible to repurpose compatible wireless-charging devices for spatial sensing while preserving their intended role in power delivery.

Turning Qi discovery pings into reliable position estimates presents three challenges. First, the pings are weak, intermittent, and transmitter-dependent, making them difficult to capture with a receiver that meets the size and power constraints of an object-mounted tag. Second, pings from multiple nearby chargers can overlap within a sensing window, so the receiver must separate their contributions to recover transmitter-specific measurements. Third, commodity chargers produce fields that depart from ideal magnetic-dipole models. Coil geometry, shielding, PCB layout, parasitic effects, and nearby materials distort the field distribution, making simple analytical models inaccurate. Localization therefore requires a calibrated model that captures these hardware-dependent fields and supports reliable inference from sparse measurements.

We present PowerTrace, a system that addresses these challenges through compact magnetic sensing, period-based signal separation, and physics-informed field modeling. A three-axis low-frequency (LF) receiver captures weak Qi pings and measures their received signal strength (RSSI). PowerTrace exploits differences in transmitter ping periods to separate concurrent chargers through period-aligned averaging, producing stable per-transmitter features. It then uses a physics-informed neural network to learn a forward map from relative position to these features. During localization, it searches for the position whose predicted features best match the measurements. The design, shown in Fig. 1, supports three modes: *probe mode*

979-8-3195-0167-7/26/$31.00 ©2026 IEEE

localizes tagged objects using fixed charger anchors; *listen mode* localizes an unmodified reverse-charging phone using fixed receivers; and *peer-to-peer (P2P) mode* estimates the distance between a transmitting phone and a second phone equipped with an LF receiver.

We implement PowerTrace using commodity Qi transmitters and compact LF sensing tags. In a controlled 100 cm × 50 cm × 50 cm workspace, the prototype achieves median 3D errors of 5.3 cm in probe mode and 4.1 cm in listen mode, with corresponding 90th-percentile errors of 11.3 cm and 9.9 cm. Phone-to-phone ranging experiments cover separations from 10 to 70 cm, with accuracy degrading near the upper end of this range. Localization remains usable under the tested non-metallic occlusions, while steel increases error. These results demonstrate the feasibility of reusing wireless-charging pings for localization in calibrated, short-range workspaces with compatible hardware. This paper makes four contributions:

- We introduce a short-range localization modality based on wireless-charging discovery pings, enabling unmodified commodity Qi charging pads and reverse-charging smartphones to serve as opportunistic magnetic beacons for localization.
- We develop a compact sensing front end for acquiring Qi discovery pings under practical constraints on form factor, circuit tuning, and receiver orientation. Our signal-processing pipeline then estimates ping periods, separates signals from concurrent transmitters through period-aligned averaging, and extracts transmitter-specific RSSI features.
- We develop a physics-informed neural network that models the asymmetric, hardware-dependent fields of commodity chargers and supports inverse localization by matching measured RSSI features to predicted values.
- We implement and evaluate the complete system across tagged-object localization, unmodified-phone localization, and phone-to-phone ranging, characterizing localization accuracy, the impact of occluding materials, and power consumption.

II. Overview

A. Wireless Power Transfer Background

Wireless power transfer (WPT) delivers energy without a wired connection, typically through near-field magnetic induction. An alternating current in a transmitter coil generates a time-varying magnetic field that induces voltage in a nearby receiver coil. The field is spatially localized, so its strength depends strongly on the receiver's position and orientation.

Qi is the dominant wireless charging standard for consumer electronics [3], [4]. Idle Qi transmitters periodically emit short discovery signals, or *pings*, to detect nearby receivers. These pings typically operate in the low-frequency magnetic-induction band within the range of 110–205 kHz [5]. Vendor reference designs also support configuring ping timing in software [6], [7]. Qi-compatible chargers are deployed at consumer scale, and smartphones also support wireless charging. Most smartphones can receive wireless power, while a growing number can charge other devices, such as earbuds, through a feature commonly called Battery Share.

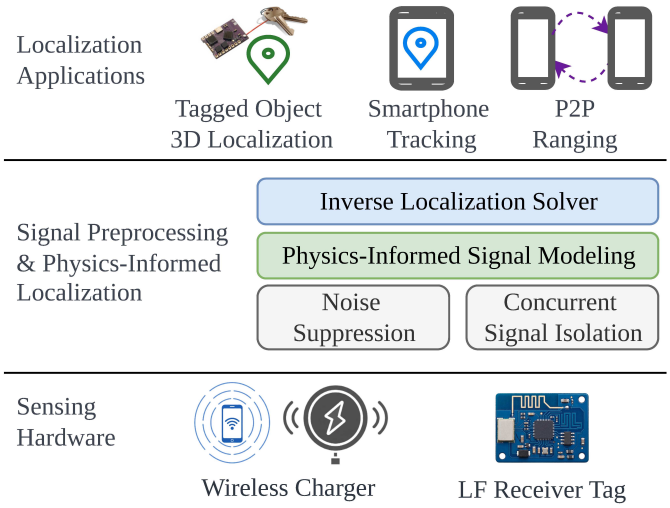


Fig. 1. PowerTrace System Overview

B. Key Intuition and Challenges

Our key intuition is that wireless-charging pings can serve as ambient near-field beacons for 3D localization. As wireless charging becomes more common in phones, charging pads, vehicles, and furniture, many commodity transmitters already emit discovery pings into their surroundings. These low-frequency magnetic signals can penetrate common non-metallic materials and are less affected by far-field multipath than RF signals. Measuring their strength reliably could therefore enable short-range indoor localization with compatible transmitters and compact LF receivers or tags.

Initial experiments (Section III) support this intuition: compact sensors can capture Qi pings whose measured magnetic-field strength varies systematically with receiver position. Translating these measurements into accurate position estimates, however, presents three challenges. First, receivers must detect weak near-field magnetic signals while remaining compact enough to attach to phones or other everyday objects. Second, pings from multiple nearby chargers may occur within the same sensing window, requiring transmitter-specific measurements to be disentangled from mixed observations. Finally, coil geometry, shielding, and device layout create asymmetric magnetic fields in practical Qi hardware, rendering idealized dipole models insufficient for accurate localization.

C. Solution Overview

PowerTrace operates in four stages (Fig. 1). First, a compact three-axis receiver captures low-frequency magnetic pings. Second, PowerTrace estimates each candidate transmitter's ping period and applies period-aligned averaging to extract transmitter-specific RSSI features from mixed, noisy observations. Third, a physics-informed forward model predicts measurements at candidate positions while accounting for the non-ideal fields of commodity chargers. Finally, PowerTrace searches the calibrated sensing volume for the position whose predicted features best match the measured RSSI.

This pipeline supports three operating modes. In probe mode, a compact LF tag attached to the target object measures

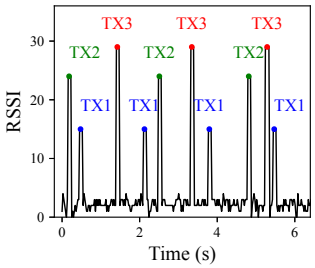


Fig. 2. Sample Measurements

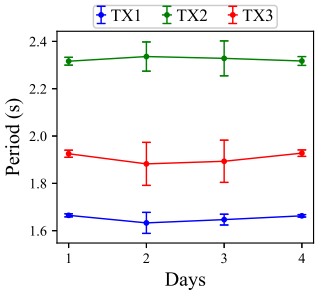


Fig. 3. Transmitters Drift

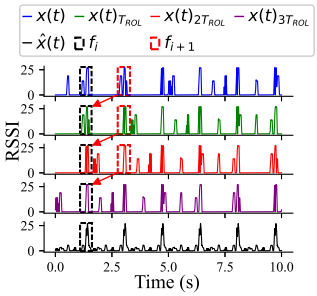


Fig. 4. Period Averaging

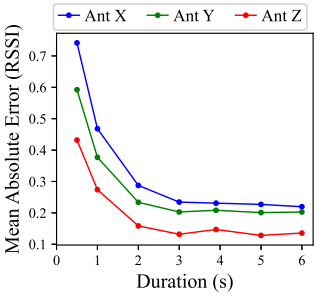


Fig. 5. RSSI Error

pings from nearby chargers at known, fixed positions. In listen mode, multiple fixed LF receivers at known positions localize an unmodified reverse-charging phone in 3D using its pings. In P2P mode, one phone emits pings and another, equipped with a compact LF tag, estimates their separation distance. Full 3D localization requires spatially distinct signal constraints from multiple chargers in probe mode or multiple receivers in listen mode. A single short-range link, as in P2P mode, supports phone-to-phone distance estimation.

Each transmitter undergoes a one-time calibration in the target workspace to learn the forward map from relative position to measured signal features. Inference then uses only standard wireless-charging discovery pings, with no changes to the Qi transmitter hardware or protocol.

III. Wireless Charging Signal Processing

PowerTrace converts raw LF RSSI samples into transmitter-specific localization features. Fig. 2 shows pings from three transmitters with similar amplitudes, occasional overlap, and substantial noise, but distinct periods of approximately 1666, 2312, and 1919 ms. The ping periods of the transmitters fluctuate slightly over different days, as illustrated in Fig. 3. Peak detection alone therefore cannot distinguish transmitters, collisions, and noise. PowerTrace instead uses period-aligned averaging. For each candidate transmitter, it folds the RSSI trace by the transmitter's ping period and averages samples at equal phases. Target pings reinforce, while unrelated pings, drift, and noise diminish.

For each antenna axis a, the algorithm first upsamples the raw sequence $x_a(t)$ by $100\times$. Although upsampling does not add information, it reduces alignment errors caused by the receiver's coarse 40 Hz sampling rate. PowerTrace then refines each nominal period T_i' by computing the Welch power spectrum and searching near the expected repetition frequency $1/T_i'$. The inverse of the dominant local peak yields the refined period T_i. This estimates the pulse repetition rate, rather than the 100–200 kHz Qi carrier frequency.

Third, PowerTrace folds the trace modulo T_i and averages same-phase samples. As shown in Fig. 4, the folded waveform for transmitter TX_i and antenna axis a is

$$\bar{x}_{i,a}(\tau) = \frac{1}{K_i(\tau)} \sum_{k=0}^{K_i(\tau)-1} x_a(\tau + kT_i), \quad \tau \in [0, T_i), \tag{1}$$

where $K_i(\tau)$ is the number of samples at phase τ in the sensing window. Components with period T_i remain aligned, while other transmitters' pings shift across phases and are suppressed by averaging. Finally, PowerTrace extracts the isolated RSSI as the maximum baseline-corrected value over one folded period:

$$s_{i,a} = \max_{\tau \in [0, T_i)} \left(\bar{x}_{i,a}(\tau) - b_{i,a} \right), \tag{2}$$

where the baseline $b_{i,a}$ is the 10th percentile of $\bar{x}_{i,a}(\tau)$. Applying this procedure to every transmitter and antenna axis yields the localization model's separated RSSI feature vector.

Fig. 5 evaluates the effect of sensing duration on RSSI estimation accuracy. With a short sensing window, the average RSSI estimation error is approximately 0.7 dB. As the sensing duration increases, the error gradually decreases, reaching approximately 0.3 dB at 3 s and remaining stable thereafter. This trend arises because short sensing windows contain too few ping peaks for period-aligned averaging to effectively suppress noise and interference. A 3 s window captures approximately ten ping intervals, providing sufficient data for stable and accurate RSSI estimation.

IV. Localization Model

PowerTrace estimates receiver position by matching measured RSSI features against a learned model of the transmitter's magnetic field. Although an ideal dipole model provides a useful baseline, it cannot accurately capture the fields generated by commodity transmitters because coil geometry, shielding, PCB layout, and parasitic effects introduce substantial distortions. Fig. 7 illustrates the resulting discrepancy between dipole-model predictions and measured RSSI values. To account for these nonidealities, PowerTrace employs a physics-informed neural network (PINN) for forward field modeling and inverse localization.

A. Forward Model

For each receiver channel i, PowerTrace trains an independent network f_{θ_i} that maps the relative sensor position $\mathbf{x} = (x, y, z)$ in transmitter-centered coordinates to the corresponding magnetic-field feature:

$$\mathbf{B}^{(i)}(\mathbf{x}) = f_{\theta_i}(\mathbf{x}). \tag{3}$$

Each network is a fully connected multilayer perceptron with four 128-neuron hidden layers and hyperbolic tangent activations, whose smoothness enables the spatial derivatives used for physics-informed regularization. Fig. 6 summarizes the multi-channel architecture.

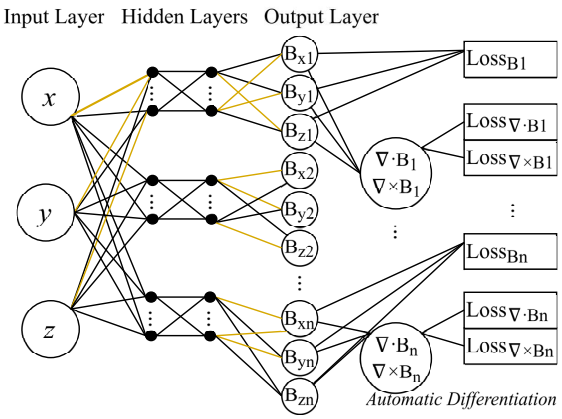


Fig. 6. Physics-Informed Neural Network Architecture

B. Training Objective

To reduce overfitting on sparse calibration samples and improve interpolation, PowerTrace combines data fitting with physics, boundary, and smoothness regularization:

$$\begin{aligned}\mathcal{L}_{total} = \mathcal{L}_{data} + \lambda_{phys}(\mathcal{L}_{div} + \mathcal{L}_{curl}) \\ + \lambda_{bnd}\mathcal{L}_{bnd} + \lambda_{smth}\mathcal{L}_{smth},\end{aligned} \tag{4}$$

where λ_{phys}, λ_{bnd}, and λ_{smth} set the relative weights.

Data-fitting loss. For calibration locations X_{gt} and measured feature $\mathbf{B}_{gt}^{(i)}(\mathbf{x})$, the supervised loss is

$$\mathcal{L}_{data}^{(i)} = \frac{1}{|X_{gt}|}\sum_{\mathbf{x}\in X_{gt}} \left\| f_{\theta_i}(\mathbf{x}) - \mathbf{B}_{gt}^{(i)}(\mathbf{x}) \right\|_2^2. \tag{5}$$

Physics-informed loss. PowerTrace uses 100–200 kHz LF signals with kilometer-scale wavelengths over meter-scale operating distances, placing the system in the quasi-static regime. Under this approximation, Maxwell's equations require the magnetic flux density $\mathbf{B}$ to satisfy

$$\begin{aligned}\nabla \cdot \mathbf{B} &= 0, \\ \nabla \times \mathbf{B} &= 0.\end{aligned}$$

We enforce these constraints at collocation points X_{col} sampled within the modeled volume. For $\mathbf{B} = (B_x, B_y, B_z)$, the divergence and the curl losses are:

$$\mathcal{L}_{div} = \frac{1}{|X_{col}|}\sum_{\mathbf{x}\in X_{col}} \left(\frac{\partial B_x}{\partial x} + \frac{\partial B_y}{\partial y} + \frac{\partial B_z}{\partial z} \right)^2, \tag{6}$$

$$\mathcal{L}_{curl} = \frac{1}{|X_{col}|}\sum_{\mathbf{x}\in X_{col}} \|\nabla \times \mathbf{B}(\mathbf{x})\|_2^2. \tag{7}$$

Automatic differentiation computes both terms, which regularize unsampled regions between sparse measurements.

Boundary loss. To discourage unrealistic extrapolation, PowerTrace samples boundary points X_{bnd} approximately 1.5 m from the transmitter, where measurements approach the noise floor, and penalizes large predicted magnitudes:

$$\mathcal{L}_{bnd} = \frac{1}{|X_{bnd}|}\sum_{\mathbf{x}\in X_{bnd}} \|\mathbf{B}(\mathbf{x})\|_2^2. \tag{8}$$

Smoothness loss. To suppress local oscillations between calibration points, PowerTrace penalizes deviations from a Gaussian-weighted average of nearby predictions. For point $\mathbf{x}_0$, neighbors $N(\mathbf{x}_0)$, and kernel scale σ,

$$\hat{\mathbf{B}}(\mathbf{x}_0) = \frac{\sum_{\mathbf{x}_j\in N(\mathbf{x}_0)} w(\mathbf{x}_0,\mathbf{x}_j) f_{\theta_i}(\mathbf{x}_j)}{\sum_{\mathbf{x}_j\in N(\mathbf{x}_0)} w(\mathbf{x}_0,\mathbf{x}_j)}, \text{where} \tag{9}$$

$$w(\mathbf{x}_0,\mathbf{x}_j) = \exp\left(-\frac{\|\mathbf{x}_0-\mathbf{x}_j\|_2^2}{2\sigma^2}\right). \tag{10}$$

The smoothness loss is

$$\mathcal{L}_{smth} = \frac{1}{|X_{smth}|}\sum_{\mathbf{x}\in X_{smth}} \left\| f_{\theta_i}(\mathbf{x}) - \hat{\mathbf{B}}(\mathbf{x}) \right\|_2^2. \tag{11}$$

Each forward model is trained on the calibration data using the Adam optimizer, with early stopping based on the loss over a held-out calibration subset. The regularization weights are fixed across all experiments. Fig. 7 compares the contributions of the model components. The dipole baseline fails to capture the asymmetry of the measured field, whereas the baseline PINN (orange) fits the calibration samples but exhibits unrealistic extrapolation near the boundary. Adding the boundary loss (green) encourages the field to decay beyond the effective sensing range but may leave local fluctuations. Combining the boundary and smoothness losses (red) produces a smoother profile that more closely follows the ground truth and decays more realistically with distance.

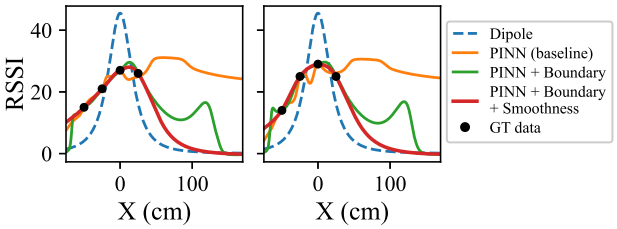


Fig. 7. Dipole Baseline vs. PINN Field Prediction

C. Localization

After training, PowerTrace freezes the feature-specific models and finds the position whose predictions best match the measurements. For measured feature $\mathbf{B}_{meas}^{(i)}$ and N available features, the estimate is

$$\mathbf{x}^* = \arg\min_{\mathbf{x}\in\Omega} \sum_{i=1}^{N} \left\| f_{\theta_i}(\mathbf{x}) - \mathbf{B}_{meas}^{(i)} \right\|_2^2, \tag{12}$$

where Ω is the calibrated sensing volume. During inference, PowerTrace solves Eq. 12 within this volume and reports the minimizer. Fig. 8 shows representative results across several

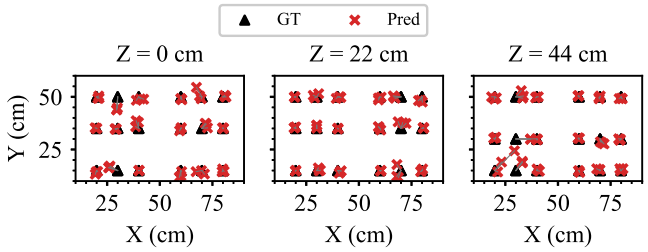


Fig. 8. Sample 3D Localization Results

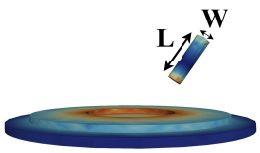


Fig. 9. Antenna Model

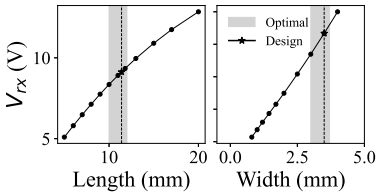


Fig. 10. Simulated Received Signal Strength vs. Core Dimensions

heights: errors are below 5 cm in many cases, with a few outliers approaching 15 cm at a height of 44 cm.

V. Application Design and Implementation

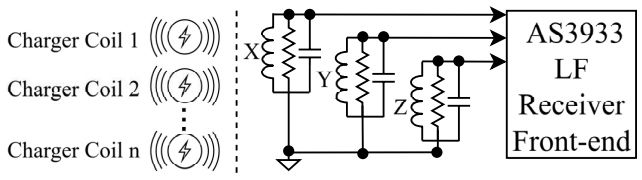
A. Hardware Design

Antenna Design. The receiver antenna must be tuned to the Qi ping band near 125 kHz, provide sufficient sensing sensitivity, and fit within the tag's form-factor constraints. Breadboard-compatible coils with inductances ranging from 1–30 mH failed to provide sufficiently high quality factors within the required footprint. Because compact LF antennas are typically available in SMT packages, which complicate iterative prototyping, we combine targeted experiments with SMT components and finite-element-method (FEM) simulations to characterize how antenna parameters affect signal quality.

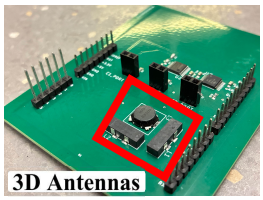
Our simulation baseline is the 7.2 mH coil used on all three sensing axes, with its geometry parameterized by axial length L and core width W (Fig. 9). In ElmerFEM, we model a ferrite-wound receiver above a current-driven Qi transmitter and represent the receiver inductor as an area-equivalent cylinder. The core and winding dimensions are derived from the manufacturer's package data. The ferrite core has an effective relative permeability of $\mu_r = 754$, consistent with MnZn ferrite behavior near 125 kHz [8], while the winding is modeled as a stranded coil using ElmerFEM's CircuitsAndDynamics formulation [9].

The parameter sweep shows a trade-off between sensitivity and size: signal strength increases with core length until it spans the dominant flux region, then saturates; increasing core width captures more flux, yielding nearly linear gains. Balancing size, quality factor, and signal strength gives the shaded design region in Fig. 10. We select 12 mH antennas for the x and y axes and 10 mH for z (vertical lines). Each RLC front end is tuned near 125 kHz: capacitance and antenna inductance set resonance, while resistance controls damping. We choose 68 pF and 220 kΩ to balance frequency selectivity, noise suppression, and RSSI sensitivity.

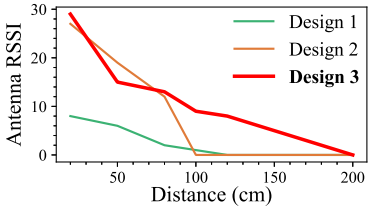
Front End IC. Software-defined radios are flexible but too bulky and power-intensive for a compact tag. We instead adapt the AS3933 LF wake-up receiver [10] to measure Qi ping RSSI along three orthogonal axes. The receiver listens continuously at the charger's 125 kHz ping frequency with packet decoding disabled (Fig. 11a). A microcontroller reads per-axis RSSI for signal processing and localization.



(a) Front End LF Receiver Design



(b) PCB Implementation



(c) Antenna RSSI vs. Distance

Fig. 11. PowerTrace Front End Design & Implementation

Hardware Prototype. Our custom PCB integrates the sensing front end, antennas, microcontroller, and supporting circuitry. The current prototype, developed over three iterations, is credit-card sized (Fig. 11b). The AS3933, antennas, and microcontroller have footprints of 36 mm, 20 mm, and 2.6 mm, respectively, leaving substantial scope for miniaturization by removing debugging headers and compacting the layout. Among the three antenna iterations in Fig. 11c, design 3 (red) provides the strongest RSSI and longest detection range.

B. Operating Mode and Application Design

PowerTrace targets calibrated, object-centric workspaces around compatible wireless-charging devices. All three modes combine compact LF ping acquisition, transmitter-specific RSSI extraction, and position or distance estimation using the learned forward model. They differ in the ping source, receiver placement, and output: 3D position or 1D distance (Fig. 12).

Probe Mode for Tagged-Object Localization. Probe mode (Fig. 12(a)) uses commodity chargers as fixed magnetic anchors and attaches a compact LF receiver to the object being localized. In our prototype, three chargers placed at known, spatially distinct locations provide complementary measurements for 3D localization. This configuration is well suited to instrumented shelves, desks, tool racks, and storage spaces equipped with wireless chargers. Each tag measures charger pings locally, so the chargers require neither data exchange nor transmission synchronization. Their ping periods, however, must be sufficiently distinct for period-aligned isolation to recover transmitter-specific features.

Listen Mode for Smartphone Localization. Listen mode (Fig. 12(b)) estimates the 3D position of a target phone using its reverse-charging pings, which are captured by multiple fixed LF receivers. It requires Battery Share to be enabled and LF receivers to be installed around the workspace, but requires no modification to the phone hardware or charging protocol. This mode is best suited to locating phones within bounded spaces, such as desks, shelves, or vehicle consoles, rather than continuous building-wide tracking.

P2P Mode for Peer Ranging. P2P mode (Fig. 12(c)) estimates the separation between a phone emitting discovery pings

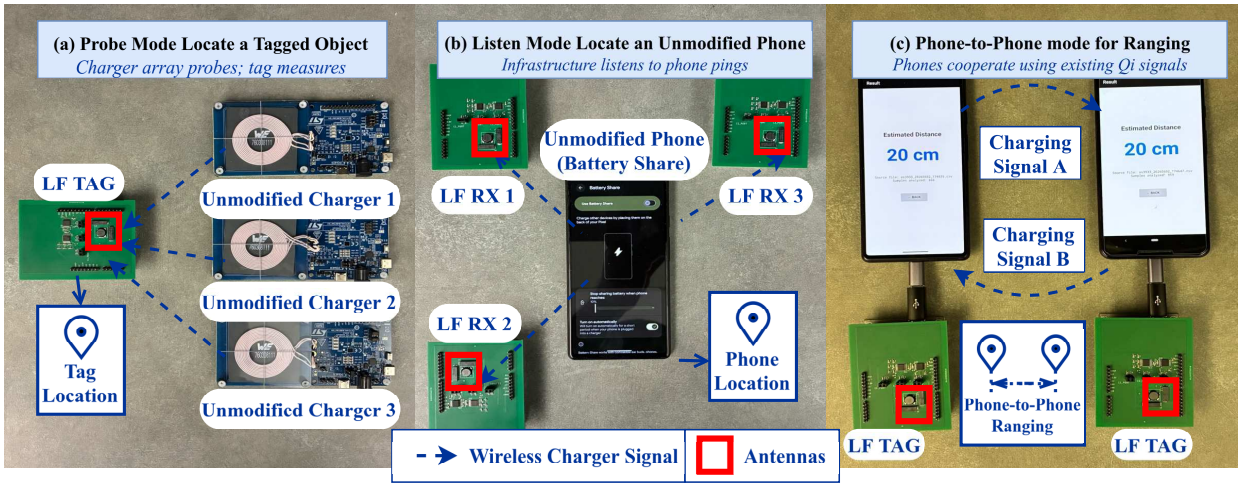


Fig. 12. PowerTrace operating modes: (a) probe mode, (b) listen mode, and (c) P2P mode

and a second phone equipped with an LF receiver, enabling short-range proximity detection and cooperative ranging. We evaluate this mode over distances of 10–70 cm and observe reduced accuracy toward the upper end of this range.

VI. Evaluation

A. Experiment Setup

We conducted all experiments in an indoor office. Probe mode used three fixed WBC86TX wireless chargers and one mobile receiver tag (Fig. 13a). Listen mode used an unmodified Google Pixel 6 Android smartphone as the ping source and three fixed receiver tags (Fig. 13b). We measured 3D ground-truth positions with a ruler and evaluated tracking accuracy and robustness on cardboard, wood, and metal shelves within a 100 cm $\times$ 50 cm $\times$ 50 cm sensing volume. We collected measurements at 126 distinct 3D coordinates across multiple sessions, moving and returning the target to each ground-truth location between sessions to improve reproducibility and reduce session-specific bias.

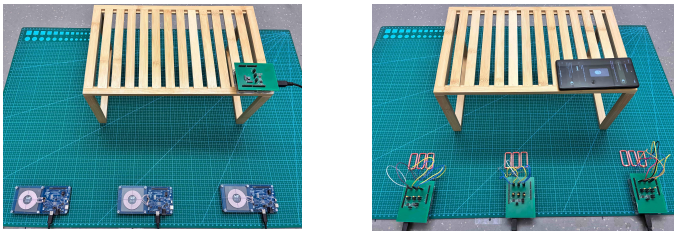
For training, we uniformly selected one sample from each of 81 locations. The remaining 1386 samples form a disjoint test set spanning all 126 locations, including 45 coordinates excluded from training. The split therefore separates samples, with the 45 held-out coordinates additionally testing interpolation and generalization to unseen locations.

B. Localization Accuracy

Localization Error Cumulative Distribution. Fig. 14 shows the 3D localization error CDFs. Probe mode (PM, green) achieves median and 90th-percentile errors of 5.3 cm and 11.3 cm, respectively; listen mode (LM, blue) achieves 4.1 cm and 9.9 cm. The same signal-processing, forward-modeling, and inverse-localization pipeline supports both deployment geometries with mode-specific calibration and minor parameter adjustments: probe mode tracks an object-mounted LF receiver, while listen mode tracks a smartphone emitting wireless-charging pings.

Listen mode performs slightly better in our setup because the Pixel 6 Battery Share implementation emits pings at approximately 3 Hz, compared with 0.5–0.7 Hz for the probe-mode chargers, providing more events to average per sensing window. At target heights of $z = 0$, 22, and 44 cm above the ground plane, both modes exhibit largely consistent error distributions (Fig. 14), indicating that PowerTrace preserves accuracy across the 3D sensing volume without relying on a fixed 2D plane.

Localization Error Distribution. A few-centimeter estimate often suffices to find a phone on a desk or an object on a shelf. We therefore also report the fractions of estimates within practical error thresholds. Fig. 15 groups errors into below 5 cm, 5–10 cm, and above 10 cm across modes and heights. In probe mode, 83%, 95%, and 86% of estimates fall below 10 cm at $z = 0$, 22, and 44 cm, respectively; the corresponding fractions within 5 cm are 44%, 60%, and 38%. Performance is best at $z = 22$ cm, where only 5% of estimates exceed



(a) Tag Tracking Experiment (b) Phone Tracking Experiment

Fig. 13. Experiment Setups

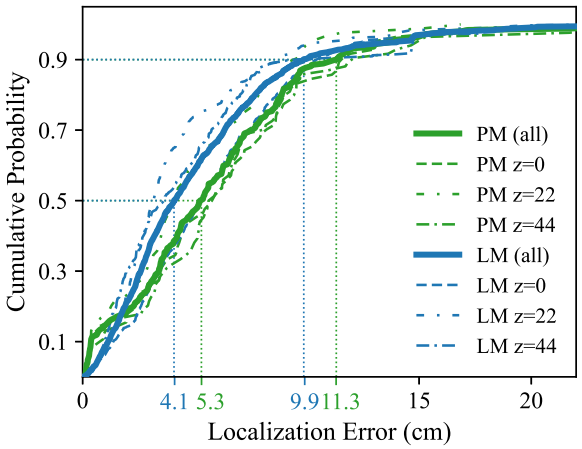


Fig. 14. 3D Localization Error CDF

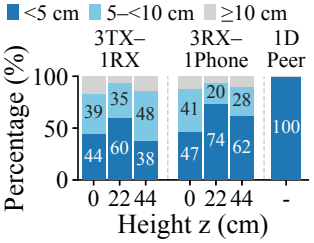


Fig. 15. Error Distribution

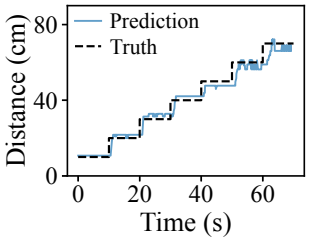


Fig. 16. P2P Dist. Estimation

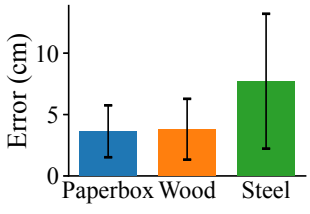


Fig. 17. Errors w. Occlusion

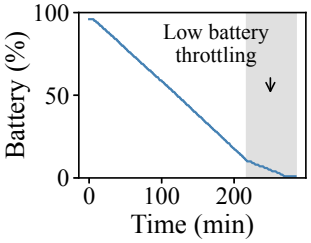


Fig. 18. Battery Drain

10 cm. Listen mode achieves similarly strong performance: at $z = 0$, 22, and 44 cm, respectively, 88%, 94%, and 90% of estimates fall below 10 cm, while 47%, 74%, and 62% fall below 5 cm. The 1D peer-to-peer ranging baseline places 100% of estimates below 5 cm, as expected for the simpler task of estimating distance rather than 3D position. Across modes and heights, these results narrow the target location to a small, practical search region.

Phone-to-Phone Ranging. We evaluate phone-to-phone ranging using a Pixel 6 in Battery Share mode as the transmitter and a phone-mounted LF receiver. In the staircase experiment (Fig. 16), separation increases from 10 to 70 cm, and the predicted distance closely follows ground truth over most of the trajectory. Tracking remains stable with minor fluctuations up to about 60 cm. At 70 cm, weaker pings near the phone's effective magnetic-field range limit increase error. The prototype thus supports ranging across the tested distances, with reduced accuracy near the range edge.

Impact of Occluding Materials. We evaluate localization with the sensor tag on paper-box, wood, and steel shelves (Fig. 17). The tested non-metallic materials have little impact on accuracy, with mean errors around 4–5 cm. Steel increases the mean error to around 8 cm and produces greater variation across trials, consistent with the attenuation and distortion of low-frequency magnetic fields by metallic materials, which destabilize received signal features [11], [12]. Even with steel, accuracy remains practical for shelf-scale object finding and coarse placement monitoring in this setup. PowerTrace remains usable under the tested non-metallic occlusions, although conductive or metallic structures pose greater challenges.

Power Consumption. We measure battery consumption on a Pixel 6 running listen mode continuously with a 15-second sensing cycle. Battery level decreases nearly linearly from 96% to 0% over 270 minutes, averaging 20.2% per hour (Fig. 18). Low-battery throttling reduces the discharge rate after about 218 minutes. Battery Historian attributes 53.66% of device power consumption to the sensing application and the remainder to the display and system processes.

C. Discussion

Wireless Charging Availability. Wireless charging is increasingly available, but PowerTrace's required infrastructure is not universal. Tagged-object localization needs multiple chargers with distinguishable ping patterns. Some environments may have only one charger coil, and some commercial chargers may lack manufacturer-accessible interfaces for configuring ping behavior. Listen and phone-to-phone modes require reverse charging, which is gaining popularity but remains unavailable on some smartphones. Additional commodity chargers can enable 3D localization in sparse deployments; a single transmitter can still support one-dimensional ranging or coarse proximity detection.

Calibration and Device Diversity. PowerTrace requires calibration to learn the mapping from position to RSSI because coil geometry, shielding, PCB layout, and parasitic coupling produce device-dependent, non-ideal fields. Physics-informed modeling improves interpolation within the calibrated volume but does not remove this requirement. Our evaluation demonstrates feasibility with a limited set of chargers, receiver tags, and a Pixel 6 Battery Share configuration. Broader deployment requires evaluation across more charger and phone models, coil geometries, furniture layouts, and environmental conditions.

Operating Range. The prototype reliably localizes within a 100 cm × 50 cm × 50 cm workspace. Even with our best receiver antenna, commodity charging pings become difficult to detect beyond roughly 2 m (Fig. 11c), limiting the current system's range. Follow-up experiments with a low-cost LF transmitter at the same 125 kHz frequency and a similar periodic ping pattern demonstrate signal capture at distances of at least 4 m. Although quasi-static near-field magnetic signals decay rapidly with distance [11], [13], this result suggests that the current range limit is not inherent to the sensing pipeline alone. Improving receiver sensitivity, antenna tuning, and signal processing may extend localization range, making longer-range LF localization a promising direction for future work.

VII. Related Work

Wireless Power and Magnetic Localization. Wireless-power systems have modeled magnetic coupling for power delivery, beamforming, integrated charging and sensing, peer-to-peer energy transfer, and side-channel analysis [12]–[16]. PowerTrace differs in both objective and signal source: it treats commodity Qi discovery pings as opportunistic short-range magnetic beacons rather than optimizing power transfer or exploiting leakage during charging. Because these pings are weak and distorted by charger-specific coil geometry, shielding, and circuit layout, PowerTrace combines compact LF sensing, period-aligned averaging for concurrent transmitters, and a physics-informed learned forward model.

Smart Shelf Sensing. Smart-shelf systems commonly rely on RFID readers and tagged products to identify items and estimate their approximate shelf locations [17]–[19]. RFID-based

approaches can exploit RSSI, phase, tag readability, reference tags, or interference patterns, but their performance is sensitive to multipath, tag orientation, dense placement, and reader configuration. Other systems use load cells, weight-change detection, or camera-assisted sensing, introducing trade-offs among spatial resolution, deployment complexity, privacy, and line-of-sight requirements [20], [21]. PowerTrace complements these approaches by using commodity Qi chargers as low-frequency magnetic beacons and compact receiver tags to measure Qi discovery pings for short-range, object-centric position estimation.

Phone-to-Phone Ranging. Phone-to-phone ranging has been studied using RF, UWB, acoustic, and vision-based signals. Bluetooth and WiFi RSSI are widely available but coarse under blockage, multipath, antenna orientation changes, and device heterogeneity [22], [23]. WiFi RTT and UWB provide more direct time-of-flight measurements, but require compatible radios, protocol support, and favorable propagation [24], [25]. Acoustic systems such as BeepBeep avoid specialized radios but require active probing and are sensitive to noise, occlusion, and audio hardware behavior [26]; vision requires line-of-sight and raises usability and privacy concerns. PowerTrace explores a complementary near-field modality by reusing low-frequency magnetic pings from phones with reverse wireless charging or Battery Share.

VIII. Conclusion and Future Work

PowerTrace repurposes Qi discovery pings for short-range localization through compact LF sensing, period-aligned transmitter separation, and RSSI-based position estimation with a physics-informed field model. The prototype localizes tagged objects and unmodified phones with low-centimeter median 3D error in controlled shelf- and desk-scale workspaces, remains usable under tested non-metallic occlusions, and supports phone-to-phone ranging. Operating range, transmitter-specific calibration, and hardware compatibility remain limitations. Future work will improve receiver sensitivity and tag integration, transfer calibration across charger models, and evaluate more devices and environments. PowerTrace demonstrates that wireless-power infrastructure can support spatial sensing alongside energy delivery.

Acknowledgment

This work is supported by the U.S. National Science Foundation under Grant No. 2502174.

References

[1] F. Zafari, A. Gkelias, and K. K. Leung, "A survey of indoor localization systems and technologies," *IEEE Communications Surveys & Tutorials*, vol. 21, no. 3, pp. 2568–2599, 2019.

[2] T. Chahoud, L. M. Amorosa, R. Marini, and L. De Nardis, "Improving outdoor multi-cell fingerprinting-based positioning via mobile data augmentation," 2025.

[3] Wireless Power Consortium, "History of the Qi Specifications," https://www.wirelesspowerconsortium.com/knowledge-base/qi-specification/history-of-the-qi-specifications/, 2026, accessed: 2026-06-19.

[4] ——, "Qi2 25W – The First Standard to Enable Truly High-Speed Qi Certified Wireless Charging," https://www.wirelesspowerconsortium.com/about-us/news-events/, 2026, accessed: 2026-06-19.

[5] Texas Instruments, *bq500210 Qi Compliant Wireless Power Transmitter Manager Datasheet*, Texas Instruments, Sep. 2012. [Online]. Available: https://www.ti.com/lit/gpn/bq500210

[6] NXP Semiconductors, *WCT1012VLF/WCT1013VLH Consumer MP-A11 (WCT-15W1CFFPD) V1.0 Wireless Charging Application User's Guide*, NXP Semiconductors, May 2019. [Online]. Available: https://www.nxp.com/docs/en/user-guide/WCT101XV10AUG.pdf

[7] Microchip Technology Inc., *Wireless Power Development Board User's Guide*, Microchip Technology Inc., 2017.

[8] T. Tsutaoka, T. Kasagi, and K. Hatakeyama, "Magnetic field effect on the complex permeability for a Mn–Zn ferrite and its composite materials," *Journal of the European Ceramic Society*, vol. 19, no. 6–7, pp. 1531–1535, 1999.

[9] E. Takala *et al.*, "Parallel simulations of inductive components with Elmer," *Electromagnetics*, vol. 36, no. 3, pp. 167–185, 2016.

[10] *AS3933 3D Low Frequency Wakeup Receiver – Data Sheet*, AMS AG, 2013. [Online]. Available: https://www1.futureelectronics.com/doc/AUSTRIAMICROSYSTEMS/AS3933-BQFT.pdf

[11] T. E. Abrudan, Z. Xiao, A. Markham, and N. Trigoni, "Distortion rejecting magneto-inductive three-dimensional localization (magloc)," *IEEE Journal on Selected Areas in Communications*, vol. 33, no. 11, pp. 2404–2417, 2015.

[12] H. Guo, Z. Sun, J. Sun, and N. M. Litchinitser, "M^2I: Channel modeling for metamaterial-enhanced magnetic induction communications," *IEEE Transactions on Antennas and Propagation*, vol. 63, no. 11, pp. 5072–5087, 2015.

[13] J. Jadidian and D. Katabi, "Magnetic MIMO: How to charge your phone in your pocket," in *Proceedings of the 20th Annual International Conference on Mobile Computing and Networking (MobiCom)*, 2014, pp. 495–506.

[14] H. Bae *et al.*, "Design of an integrated near-field communication and wireless power transfer coupler for mobile device applications," *Technologies*, vol. 13, no. 5, p. 207, 2025.

[15] P. Yang, A. Abusafia, A. Lakhdari, and A. Bouguettaya, "Towards peer-to-peer sharing of wireless energy services," arXiv:2211.12464, 2022.

[16] T. Ni *et al.*, "Uncovering user interactions on smartphones via wireless charging side channels," in *2023 IEEE Symposium on Security and Privacy (SP)*, 2023, pp. 3399–3415.

[17] J. S. Choi, H. Lee, D. W. Engels, and R. Elmasri, "Passive uhf rfid-based localization using detection of tag interference on smart shelf," *IEEE Transactions on Systems, Man, and Cybernetics, Part C (Applications and Reviews)*, vol. 42, no. 2, pp. 268–275, 2012.

[18] M. R. Souryal, D. K. Ljungberg, L.-A. King, and J. Mehrens, "RFID-based localization and tracking technologies," *IEEE Pervasive Computing*, vol. 10, no. 1, pp. 45–51, 2011.

[19] A. Papapostolou and H. Chaouchi, "RFID-assisted indoor localization and the impact of interference on its performance," *Journal of Network and Computer Applications*, vol. 34, no. 3, pp. 902–913, 2011.

[20] J. Falcão, C. Ruiz, S. Pan, H. Y. Noh, and P. Zhang, "Faim: Vision and weight sensing fusion framework for autonomous inventory monitoring in convenience stores," *Frontiers in Built Environment*, vol. 6, p. 568372, 2020.

[21] J. A. C. Jose, C. J. B. Bertumen, M. T. C. Roque, A. E. B. Umali, J. C. T. Villanueva, R. J. TanAi, E. Sybingco, J. San Juan, and E. C. Gonzales, "Smart shelf system for customer behavior tracking in supermarkets," *Sensors*, vol. 24, no. 2, p. 367, 2024.

[22] T. Lovett, M. Briers, M. Charalambides, R. Jersakova, J. Lomax, and C. Holmes, "Inferring proximity from Bluetooth Low Energy RSSI with unscented Kalman smoothers," 2020.

[23] Z. Van Hyfte and A. Zakhor, "Immediate proximity detection using Wi-Fi-enabled smartphones," 2021.

[24] C. Ma, B. Wu, S. Poslad, and D. R. Selviah, "Wi-Fi RTT ranging performance characterization and positioning system design," *IEEE Transactions on Mobile Computing*, 2020.

[25] A. Heinrich, S. Krollmann, F. Putz, and M. Hollick, "Smartphones with UWB: Evaluating the accuracy and reliability of UWB ranging," 2023.

[26] C. Peng, G. Shen, Y. Zhang, Y. Li, and K. Tan, "BeepBeep: A high accuracy acoustic ranging system using COTS mobile devices," in *Proceedings of the 5th ACM Conference on Embedded Networked Sensor Systems (SenSys)*. ACM, 2007, pp. 1–14.